The AAPS Journal (2019) 21: 107
DOI: 10.1208/s12248-019-0374-2

Research Article

Inhibition of Hepatic CYP2D6 by the Active *N*-Oxide Metabolite of Sorafenib

Michael Murray,[1,4] Tina B. Gillani,[1] Tristan Rawling,[2] and Pramod C. Nair[3]

Received 21 July 2019; accepted 16 August 2019; published online 21 October 2019

Abstract. The multikinase inhibitor sorafenib (SOR) is used to treat patients with hepatocellular and renal carcinomas. SOR undergoes CYP-mediated biotransformation to a pharmacologically active *N*-oxide metabolite (SNO) that has been shown to accumulate to varying extents in individuals. Kinase inhibitors like SOR are frequently coadministered with a range of other drugs to improve the efficacy of anticancer drug therapy and to treat comorbidities. Recent evidence has suggested that SNO is more effective than SOR as an inhibitor of CYP3A4-mediated midazolam 1′-hydroxylation. CYP2D6 is also reportedly inhibited by SOR. The present study assessed the possibility that SNO might contribute to CYP2D6 inhibition. The inhibition kinetics of CYP2D6-mediated dextromethorphan *O*-demethylation were analyzed in human hepatic microsomes, with SNO found to be ~ 19-fold more active than SOR (K_Is 1.8 ± 0.3 μM and 34 ± 11 μM, respectively). Molecular docking studies of SOR and SNO were undertaken using multiple crystal structures of CYP2D6. Both molecules mediated interactions with key amino acid residues in putative substrate recognition sites of CYP2D6. However, a larger number of H-bonding interactions was noted between the *N*-oxide moiety of SNO and active site residues that account for its greater inhibition potency. These findings suggest that SNO has the potential to contribute to pharmacokinetic interactions involving SOR, perhaps in those individuals in whom SNO accumulates.

KEY WORDS: CYP2D6 inhibition; dextromethorphan O-demethylation; metabolite inhibition; molecular docking; sorafenib; sorafenib *N*-oxide.

INTRODUCTION

The multi-kinase inhibitor sorafenib (SOR) is valuable in the clinical treatment of hepatic and renal carcinomas (1,2); Fig. 1). Compared to conventional cytotoxic anticancer agents, kinase inhibitor drugs like SOR are generally well tolerated. However, dose-limiting toxicities, such as the hand-foot syndrome, and pharmacokinetic drug-drug interactions (DDIs) occur in some patients who receive SOR. These events may require dosage interruptions or the termination of SOR therapy (1–3).

Human cytochrome P450 (CYP) CYP3A4 mediates the hepatic biotransformation of SOR to its active metabolite SOR *N*-oxide (SNO; Fig. 1), which is a major pathway of SOR elimination (4,5). Pharmacokinetic studies have demonstrated wide interindividual variation in the clearance of SOR and that both SOR and SNO accumulate to varying extents in patients on repeated dosage (3,6–9). Kinase inhibitors like SOR are also now being used increasingly in combination with other drugs to achieve improved anticancer efficacy and for the treatment of coincident clinical conditions; this increases the possibility of DDIs.

In some patients, high serum concentrations of the major SOR metabolite SNO are produced (8). We found recently that CYP3A4 was inhibited more effectively by SNO than by the parent drug SOR (10), which suggests that patients that produce more SNO may be at greater risk of pharmacokinetic DDIs. The overproduction and accumulation of the metabolite SNO could also elicit DDIs involving other CYPs. Indeed, a large number of therapeutic agents are contraindicated with SOR (https://www.drugs.com/drug-interactions/sorafenib-index.html), including some that are substrates for the polymorphic CYP2D6 that mediates the oxidative elimination of many drugs. From the company literature, SOR is

[1] Pharmacogenomics and Drug Development Group, Discipline of Pharmacology, School of Medical Sciences, Faculty of Medicine and Health, University of Sydney, Sydney, NSW 2006, Australia.
[2] School of Mathematical and Physical Sciences, Faculty of Science, University of Technology Sydney, Ultimo, New South Wales 2007, Australia.
[3] Department of Clinical Pharmacology and Flinders Centre for Innovation in Cancer, College of Medicine and Public Health, Flinders University, Bedford Park, SA 5042, Australia.
[4] To whom correspondence should be addressed. (e–mail: michael.murray@sydney.edu.au)

Abbreviations: *AUC*, area under the serum concentration versus time curve; C_{max}, maximal serum concentration; *CYP*, cytochrome P450; *DDI*, drug-drug interaction; *SOR*, sorafenib; *SNO*, sorafenib *N*-oxide; *SRS*, substrate recognition site.

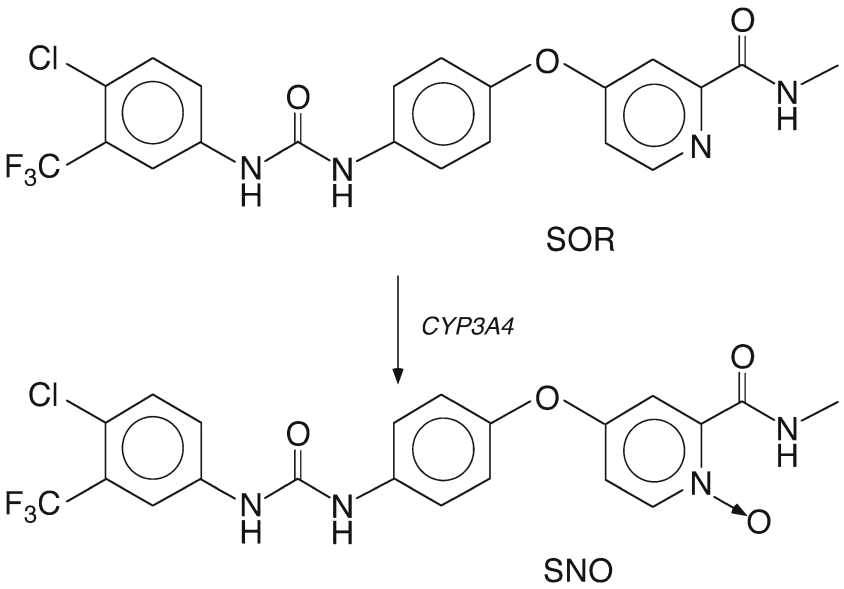

Fig. 1. SOR and its biotransformation to the principal metabolite SNO

considered to be a moderately effective inhibitor of CYP2D6 https://www.accessdata.fda.gov/drugsatfda_docs/label/2010/021923s008s009lbl.pdf, but it is presently unclear whether the metabolite SNO also inhibits this important enzyme.

The present study assessed the relative capacities of SOR and SNO to inhibit CYP2D6-mediated dextromethorphan *O*-demethylation in human liver microsomes. From kinetic studies, the principal finding to emerge was that SNO was ~ 19-fold more effective than SOR as a CYP2D6 inhibitor. In docking studies, SNO and SOR interacted with key amino acid residues in the catalytic site of CYP2D6 that are associated with ligand binding. The estimated affinity was greater for SNO than SOR because additional H-bonds were formed between active sites residues and the *N*-oxide moiety. These findings suggest that SNO has the capacity to contribute to CYP2D6 inhibition in patients who receive treatment with SOR.

MATERIALS AND METHODS

Drugs and Chemicals

The syntheses of SOR (4-[4-([4-chloro-3-(trifluoromethyl)phenyl]carbamoylamino)phenoxy]-*N*-methylpyridine-2-carboxamide) and SNO have been described previously (11). Dextromethorphan, midazolam, and biochemicals were purchased from Sigma-Aldrich (Castle Hill, NSW, Australia). [4-^{14}C]-Testosterone (37 kBq/μCi) was obtained from Perkin Elmer (Glen Waverley, VIC, Australia). 1′-Hydroxymidazolam was from Cerilliant (Round Rock, TX, USA), while other CYP metabolites were from Sigma. Microsomal fractions containing cDNA-expressed CYP2D6 in insect cells were purchased from BD Biosciences (Supersomes; North Ryde, NSW, Australia). HPLC grade solvents and general reagents were obtained from LabScan (Lomb Scientific, Taren Point, NSW, Australia) or Ajax Chemicals (Sydney, NSW, Australia).

Liver Donors and the Preparation of Microsomal Fractions

This study was reviewed and approved by the University of Sydney Human Ethics committee in accordance with the guidelines from the World Medical Association. Human hepatic microsomal fractions were prepared by ultracentrifugation (12), using tissue from three liver donors and obtained through the Australian and Queensland Liver Transplant Programs (Royal Prince Alfred Hospital, Sydney, NSW, and Princess Alexandria Hospital, Brisbane, Queensland, respectively). Small quantities of normal tissue were collected during surgical liver resection, perfused immediately with cold Viaspan solution (DuPont, Wilmington, DE, USA), and transferred to liquid nitrogen. Liver microsomal protein was quantified by established methods (13).

CYP Substrate Oxidation Assays in Human Liver Microsomes

Dextromethorphan *O*-demethylation activity was determined by LC-MS/MS, as described previously (14). Incubations (37 °C, microsomal protein 150 μg, 0–48 μM dextromethorphan, NADPH 1 mM, 30 min) were conducted in 0.1 M potassium phosphate buffer (pH 7.4; 0.25 mL). After solid-phase extraction on Bond Elut C18 cartridges (Agilent Technologies, Mulgrave, VIC, Australia) samples were applied to an Altima C_{18} 5 μ 150 × 2.1 mm column (Alltech Associates, Castle Hill, NSW, Australia) and were eluted using a mobile phase of 50% aqueous acetonitrile, containing 0.1% formic acid; the flow rate was 0.3 mL/min, and the data were analyzed using Xcalibur 1.2 (Thermo Fisher, Waltham, MA).

Microsomal SNO formation was determined by LC-MS/MS, as described previously (5). Incubations (37 °C, 75 μg protein, 75 μM SOR, NADPH 1 mM, 20 min) were conducted in 0.1 M potassium phosphate buffer (pH 7.4, 0.25 mL). After addition of acetonitrile (0.5 mL) and centrifugation (600 g, 5 min), samples were applied to an XTerra MS C18 3.5 μ column 150 × 2.1 mm column (Waters,

Rydalmere, NSW, Australia). The mobile phase was 65% aqueous acetonitrile and 0.1% formic acid, which was increased to 100% acetonitrile after 30 s, before being returned to the starting composition after 2 min; the flow rate was 0.3 mL/min and the data were analyzed using Xcalibur 1.2.

Midazolam 1′-hydroxylation was determined by LC-MS/MS, as described previously (14). Incubations (37 °C, 100 μg protein, 5 μM midazolam, 1 mM NADPH, 5 min) were conducted in 0.1 M potassium phosphate buffer (pH 7.4, 0.5 mL). After solid-phase extraction on Bond Elut C18 cartridges (Agilent Technologies) samples were applied to an Altima C_{18} 5 μ 150 × 2.1 mm column (Alltech Associates). The mobile phase was 50% aqueous acetonitrile, containing 0.1% formic acid; the flow rate was 0.3 mL/min and the data were analyzed using Xcalibur 1.2.

Testosterone hydroxylation was determined by scintillation spectrometry, as described previously (15). Incubations (37 °C, 150 μg protein, 50 μM ^{14}C-testosterone [0.18 μCi], 1 mM NADPH, 2.5 min) were conducted in 0.1 M potassium phosphate buffer (pH 7.4, 0.5 mL). After extraction with chloroform, samples were subjected to thin-layer chromatography on silica gel 60 F254 plates (20 cm × 20 cm × 0.25 mm; Merck, Darmstadt, Germany) and were then resolved in dichloromethane/acetone (4:1), followed by chloroform/ethyl acetate/ethanol (4:1:0.7); radioactive metabolites were located by autoradiography (15).

Kinetics of Inhibition of CYP2D6-Dependent Dextromethorphan *O*-Demethylation by SOR and SNO

Kinetic studies of dextromethorphan *O*-demethylation in human liver microsomes were conducted over the dextromethorphan range 0–48 μM. The kinetics of dextrorphan formation (V) as a function of dextromethorphan (S) concentration were analyzed by nonlinear regression; r^2 values were determined for all regression lines (GraphPad Prism 5; San Diego, CA). Data were analyzed further using the methods of Lineweaver-Burk and Dixon with corresponding replots to characterize the mode of inhibition (16). K_i values were obtained from the *x*-intercepts of Lineweaver-Burk slope replots. Total drug concentrations were used because these have been found to improve the assessment of DDIs with hydrophobic drugs like dextromethorphan and SOR that may accumulate in liver (17).

Computational Studies of the Docking of SOR and SNO into the Active Site of CYP2D6

To account for the structural plasticity of CYP2D6, three X-ray crystal structures (3TDA, chain A; 4WNU, chain B; 4WNV, chain A) were used in molecular docking studies. The unresolved residues in the structures, 4WNU (38-50) and 4WNV (48-50) were built using the modloop program (https://modbase.compbio.ucsf.edu/modloop/) (18). Structures were prepared by including H-atoms and Kollman all atom charges using the BioPolymer module of SYBYL (version X-2.1, Certara, Princeton, NJ, USA). Unresolved residues in the N- and C-termini of the X-ray structures, which are distant from the catalytic site, were excluded from the analysis.

Three-dimensional coordinates of SOR and SNO in sdf format were obtained from Pubchem (https://pubchem.ncbi.nlm.nih.gov/), and molecular modeling was achieved using SYBYL, installed on a Red Hat Linux 6.9 OS workstation. After assignment of Gasteiger–Huckel partial atomic charges (19), energy minimization was performed using Powell's conjugate gradient method in conjunction with a Tripos 5.2 force field (20,21). A minimum energy difference of 0.001 kcal/mol was set as the convergence criterion.

Molecular docking experiments were conducted using the Surflex-Dock docking suite (22) as previously reported (5,23). The resulting binding poses were ranked according to the total score (SYBYL Surflex-Dock). The dissociation constants (K_d) for SOR and SNO docked in CYP2D6 crystal structures were estimated as described by Pham and Jain (24).

Statistics

Data are expressed throughout as means ± SEM of individual estimates as indicated.

RESULTS

Human Liver Donors and Rates of Oxidation of Dextromethorphan and Other CYP Substrates in Microsomal Fractions

Liver tissue from 3 individual donors was available for the present study (designated HL8, HL13 and HL19). Limited information on demographic factors (age 16, gender female) and drug history (prednisone) was available for one donor (HL8), but no information was available for donors HL13 or HL19. Rates of CYP2D6-mediated dextromethorphan *O*-demethylation were quantitifed in the livers and varied over a ~ 4.4-fold range (14–61 pmol dextrorphan formation/mg protein/min; Table I). In comparison, microsomal SNO formation varied 7.5-fold in the fractions (22.4–169 pmol/mg protein/min), and midazolam 1′-hydroxylation and testosterone 6β-hydroxylation varied over ~ 7.8- and 22-fold ranges, respectively (Table I).

Kinetics of the Inhibition of Microsomal CYP2D6-Dependent *O*-Demethylation of Dextromethorphan by SOR and its Major Oxidized Metabolite SNO

The K_m value for microsomal dextromethorphan *O*-demethylation was 4.7 ± 1.0 μM (Fig. 2a), while the V_{max} for dextrorphan formation was 51 ± 19 pmol dextrorphan/min/mg protein ($n = 3$); these values are compatible with those reported previously (25). In preliminary microsomal studies, IC_{50} values of 12 ± 5 μM and > 50 μM were obtained for SNO and SOR, respectively, at a dextromethorphan concentration of 16 μM. In confirmation of these findings, the IC_{50}s for SNO and SOR against cDNA-expressed human CYP2D6 were 13 ± 1 μM and > 50 μM, respectively (not shown). Kinetic studies were done using the available livers to evaluate inhibitory mechanisms in greater detail, and the data were fitted to alternate models of inhibition (GraphPad Prism 5). The optimal fit was obtained for linear-mixed inhibition kinetics, as described by the Henri-Michaelis-Menten equation:

Table I. Substrate Oxidations in Human Liver Microsomal Fractions

Donor	Dextromethorphan *O*-Demethylation	SOR *N*-oxidation	Midazolam 1′-Hydroxylation	Testosterone 6β-Hydroxylation
	(pmol/mg protein/min)			(nmol/mg protein/min)
HL8	25	22.4	10	0.1
HL13	14	133	69	0.8
HL19	61	169	78	2.2

Values are means of at least duplicate determinations that varied by < 12%

$$\frac{V}{V_{\max}} = \frac{S}{K_m\left(1+\frac{I}{K_i}\right)+S\left(1+\frac{I}{\alpha K_i}\right)}$$

Lineweaver-Burk plots (Fig. 2b, c) and their slope replots (Fig. 2d) confirmed that the mode of inhibition for both SNO and SOR was linear-mixed (16). K_is were obtained from the *x*-intercepts on Lineweaver-Burk slope replots (Fig. 2d) and were 1.8 ± 0.3 μM and 34 ± 11 μM for SNO and SOR, respectively. The factor α describes the increase in the equilibrium constants K_m and K_i by inhibitor and substrate, respectively (16; Fig. 3); α values were 9 ± 2 and 25 ± 6 for SNO and SOR, respectively.

Computational Modeling of Docking of SOR and SNO with CYP2D6

Thirteen X-ray crystal structures of the wild-type human CYP2D6 are available with five having been derived in the presence of a bound inhibitor (quinine, quinidine, prinomastat (2 independent structures), ajmalicine). Based on the present kinetic data, it was postulated that SOR and SNO might inhibit CYP2D6 by binding in similar orientations to those noted for other inhibitors in the CYP2D6 X-ray complexes. Additionally, in view of the structural flexibility of the CYP2D6 binding site, we performed molecular docking of SOR and SNO with three CYP2D6 X-ray crystal structures that were resolved in the presence of inhibitors—3TDA (Fig. 4a, b), 4WNU (Fig. 4c, d), and 4WNV (Fig. 4e, f). Docking of SOR in the 3TDA structure revealed two key H-bonding interactions between the urea nitrogens and the carboxylate side chain of Glu 216 (Fig. 4a). In the docked pose of SOR, the trifluoromethyl-substituted phenyl ring was involved in hydrophobic/π-π interactions with Phe 120, whereas the central phenyl ring of SOR also formed π-π interactions with Phe 483. The fluorine atoms in the aromatic CF_3 group are also potential H-bond acceptors for Ser 304. The picolinamide system in SOR forms π-π interactions with the aromatic residues Phe 51, Phe 58, and Phe 481, while the O atom of picolinamide group is H-bonded with Thr 54. Other residues that line the binding site and participate in hydrophobic interactions include Val 49, Leu 71, Leu 73, Val 78, Leu 121, Leu 213, Val 308, Leu 372, Val 374, and Ile 396. The binding interactions of the docked poses of SOR in the 4WNU and 4WNV structures were similar, although there was a noticeable difference in the orientation of the picolinamide system (Fig. 4c, e). In the 4WNU structure, the amido oxygen of SOR forms H-bonds with the hydroxyl group of Thr 375 and the amido nitrogen forms H-bonds with Glu 222. Notably, Glu 216 was located further from SOR/SNO when docked with the 4WNU and 4WNV structures.

Each of the interactions above was also observed for SNO. Importantly, however, there were additional interactions that produced higher estimated binding affinities for SNO (Table II). These are calculated K_d values that were estimated from Surflex docking scores and varied between crystal structures. Although these values should be interpreted carefully they were consistently lower for SNO than for SOR. In 3TDA, the O atom of the *N*-oxide moiety of SNO was involved in additional H-bonding interactions with Thr 54 (Fig. 4b) and with Thr 394 in the 4WNU and 4WNV structures (Fig. 4d, f). In the 4WNU structure, the O atom of the picolinamide moiety is H-bonded with Thr 375 (Fig. 4d), whereas in the 4WNV structure H-bonding with Thr 76 was noted (Fig. 4f). Further, the orientations of the pyridine ring and the amide side chain of the picolinamide moiety in SNO differed somewhat from SOR in these structures. This could be due to small differences in the orientation of important amino acid side chains, such as Phe 483, to differences in secondary structure, and to the conformations of amino acids, such as residues 49–51, near the helix A in the 4WNU and 4WNVstructures.

DISCUSSION

In previous studies, SNO—the major pharmacologically active metabolite of SOR—was found to be approximately twice as potent as the parent drug as an inhibitor of CYP3A4 (10). Whereas SOR has been reported to be a moderate inhibitor of CYP2D6 (https://www.accessdata.fda.gov/drugsatfda_docs/label/2010/021923s008s009lbl.pdf), to our knowledge, inhibition of CYP2D6 by the metabolite SNO has not been evaluated in detail. In some cases, CYP-mediated drug metabolites are more effective inhibitors than the parent drugs. These include highly reactive metabolites generated during biotransformation of alkylamino, methylenedioxyphenyl, thionosulfur, phenolic, and unsaturated functional groups in some CYP substrates (26–32), as well as certain stable metabolites, including *N*-oxides, that elicit reversible inhibition of CYPs (33–36). In the present study, we assessed the possibility that the stable *N*-oxide metabolite SNO may contribute to the inhibition of CYP2D6 activity. SNO was markedly more effective than SOR as a CYP2D6 inhibitor. Dextromethorphan *O*-demethylation is widely used as a CYP2D6-selective assay in human liver

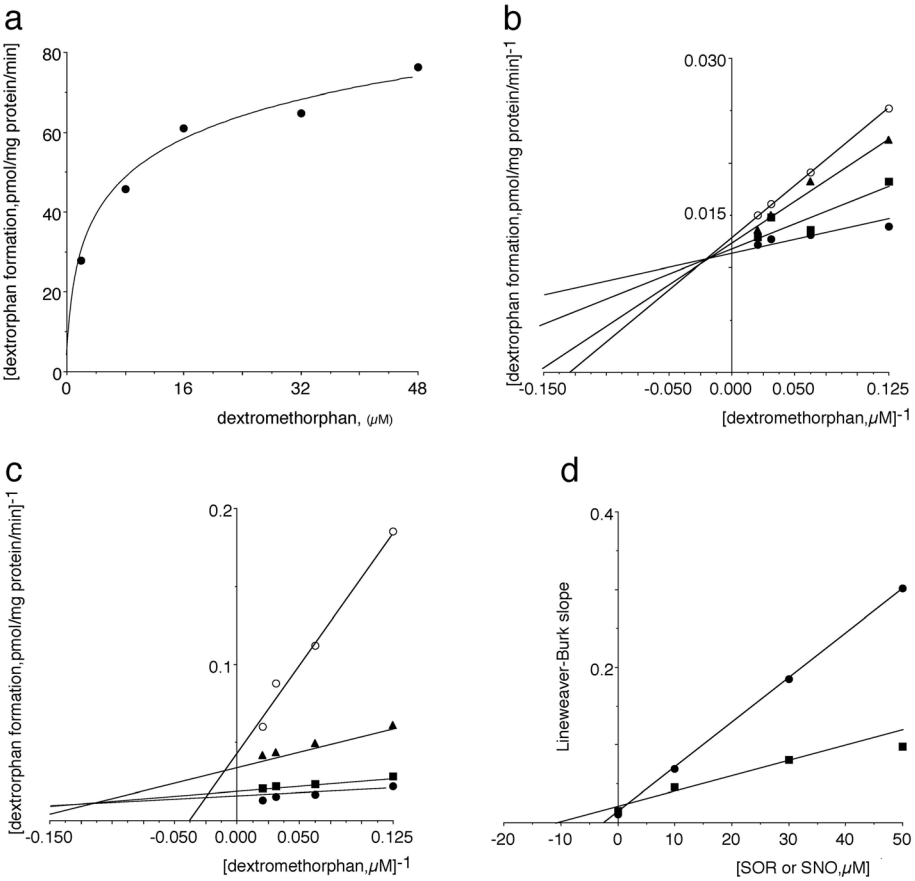

Fig. 2. Kinetic analysis of the inhibition of human microsomal CYP2D6-mediated dextromethorphan *O*-demethylation by SOR and SNO. **a** Michaelis-Menten plot of dextromethorphan *O*-demethylation. **b** Lineweaver-Burk plot at SOR concentrations (filled circles) 0 μM, (filled squares) 10 μM, (filled triangles) 30 μM, (empty circles) 50 μM. **c** Lineweaver-Burk plot at SNO concentrations (filled circles) 0 μM, (filled squares) 10 μM, (filled triangles) 30 μM, (empty circles) 50 μM. **d** Lineweaver-Burk slope replots for SOR and SNO. A representative analysis conducted in one of three individual microsomal fractions is shown. Values are means of at least duplicate determinations that varied by < 12%

microsomes and in phenotyping cocktails in vivo (14,37). We used the assay in liver microsomes because the CYP enzyme environment more closely resembles the native situation and is preferred in DDI studies (38). In contrast, heterologous systems containing over-expressed recombinant CYPs exhibit atypical ratios of CYPs to other enzymes, including NADPH-CYP-reductase, and atypical membrane compositions (38). In the present study the K_i for SNO against CYP2D6-mediated dextromethorphan *O*-demethylation was about 19-fold smaller than that for SOR, indicating greater affinity for the enzyme. Because the K_m for dextromethorphan was ~ 4.5 μM, CYP2D6 has an approximate 4-fold greater affinity for SNO than for dextromethorphan. In contrast, the affinity of CYP2D6 for dextromethorphan was ~ 8-fold that of SOR, which is consistent with the lesser inhibition potency of the latter. Accordingly, the present findings suggest that SNO is a significant reversible inhibitor of CYP2D6.

We evaluated the binding mode and binding interactions of SOR and SNO within CYP2D6 using molecular docking studies. Three X-ray crystal structures of CYP2D6 were used in order to account for CYP2D6 active site plasticity. The binding interactions of SNO and SOR across the three

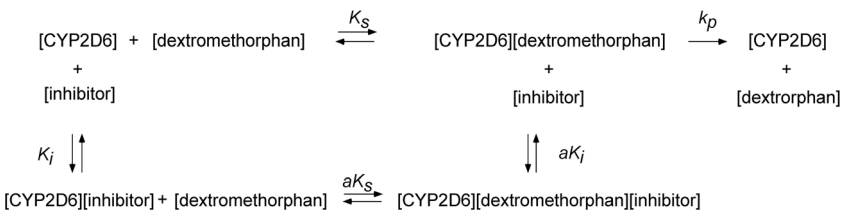

Fig. 3. Michaelis-Menten equilibria showing formation of CYP2D6-inhibitor/substrate complexes and linear mixed-type reversible inhibition of CYP2D6-dependent dextromethorphan *O*-demethylation; [inhibitor] refers to either SOR or SNO

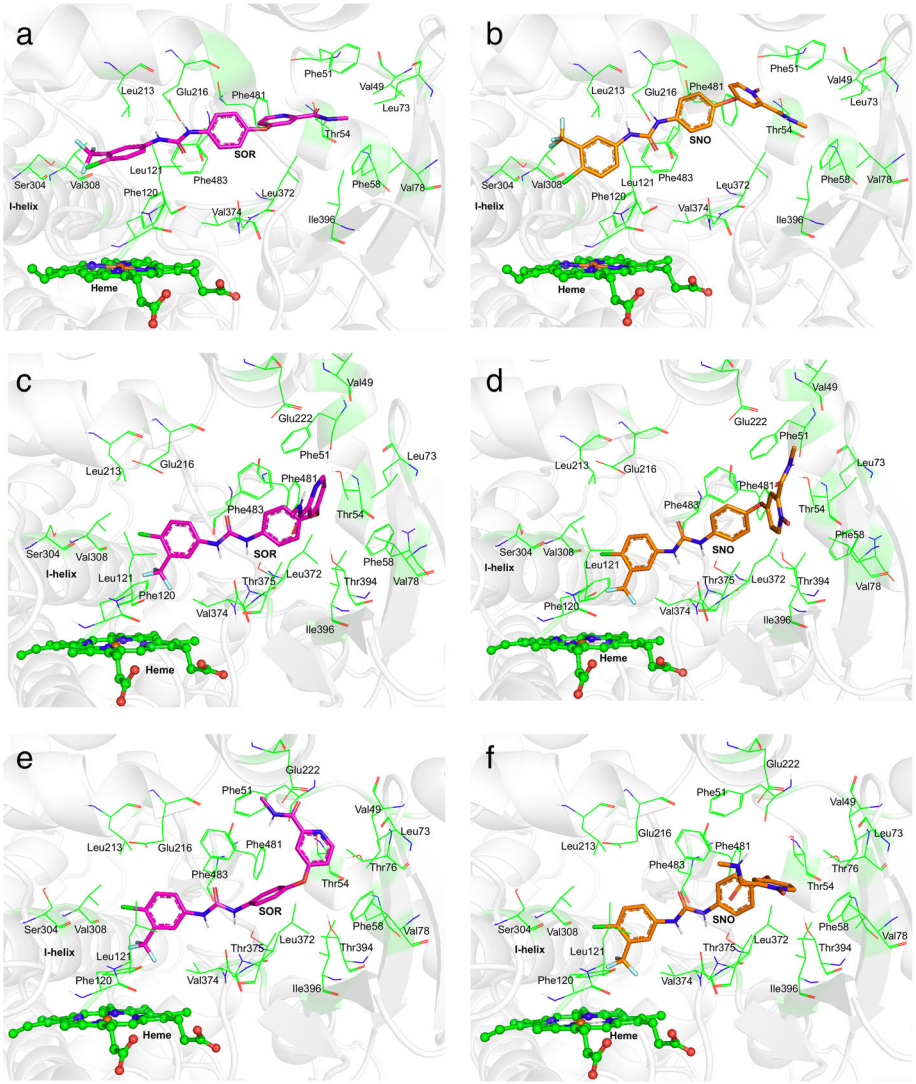

Fig. 4. Binding modes of SOR and SNO in X-ray structures of CYP2D6 enzyme, key binding site residues are displayed (C atoms in green). **a**, **b** 3TDA. **c**, **d** 4WNU. **e**, **f** 4WNV. C atoms in SOR and SNO are represented as sticks in magenta and orange, respectively. The CYP heme is shown in ball and stick format. O, N, F, and Cl are shown in red, blue, cyan, and green, respectively

structures were similar. CYP2D6 residues involved in interactions with SOR and SNO, and the location of protein helical domains, β-sheets, and putative substrate recognition sites (SRS; 39) are shown in Fig. 5.

Amino acids that interacted with SOR and SNO were located in SRS-1 (which spans residues 99–125), SRS-2 (which spans 213–219), SRS-4 (which spans 294–312), SRS-5 (which spans 369–377), and SRS-6 (which spans 481–488), but not SRS-3. In SRS-1, the residues Phe 120 and Leu 121were involved in SOR/SNO interactions, as were Leu 213 and Glu 216 from SRS-2; Ser 304 and Val 308 from SRS-4; Leu 372, Val 374, and Thr 375 from SRS-5; and Phe 481 and Phe 483 from SRS-6. A number of residues (Val 49, Phe 51, Phe 58, Thr 54, Leu 71, Leu 73, Thr 76, Val 78, Glu 222, and Thr 394) were also involved in SOR/SNO interactions but were outside SRS regions. Some of these CYP2D6 residues involved in SOR/SNO interactions have also been identified in previous homology modeling studies of the interactions with other CYP2D6 substrates and inhibitors with the enzyme. These include Glu 216 in SRS-2, Ser 304 in SRS-4, Val 374 in SRS-5, and Phe 481 and Phe 483 in SRS-6 (40–42). Glu 216 sits at the top of the active site cavity and has been proposed to be a recognition residue for basic ligands that enter the binding pocket of the enzyme. Phe 481 and Phe 483 are proposed to make hydrophobic interactions with the aromatic regions of

Table II. Estimated Binding Constants for the Interaction of SOR and SNO with CYP2D6

CYP2D6 X-ray		K_d (μM)	
Structure	SOR	SNO	SOR/SNO
3TDA	25.2	0.032	785
4WNU	0.40	0.008	50
4WNV	1.26	0.063	20

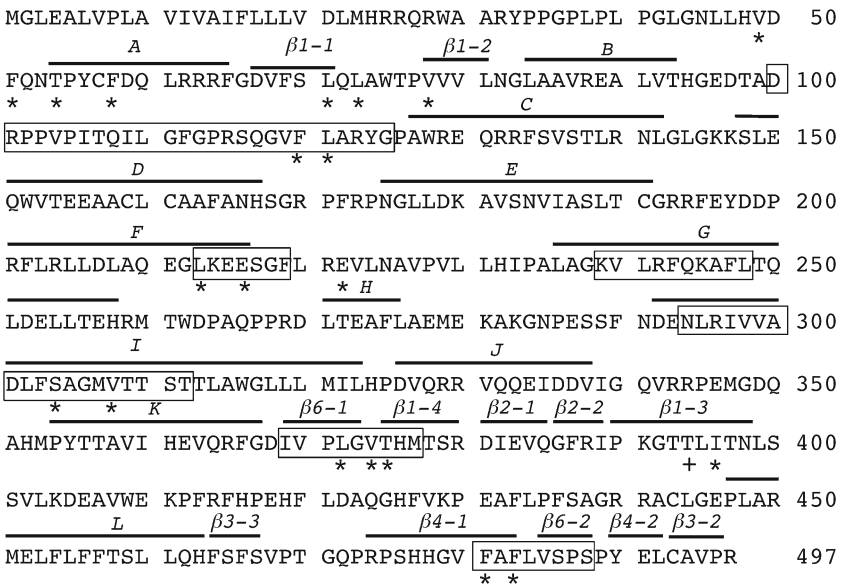

Fig. 5. Amino acid sequence of CYP2D6 showing the location of residues implicated in binding interactions with both SOR and SNO (asterisks) and SNO alone (crosses). Bars indicate the locations of helical domains and β-sheets (italicized). Amino acid residues in putative SRS regions are shown in boxes

substrates. The SRS-1 residues Phe 120 and Leu 121, SRS-2 residue Leu 213, and SRS-4 residue Ser 304 are also proposed to be involved in substrate recognition. Indeed, Phe 120 in SRS-1 reportedly controls the orientation of substrates with respect to the CYP heme catalytic center and the regioselectivity of substrate oxidation (42,43).

In the 3TDA structure H-bonding interactions were noted between the urea nitrogens of SOR and the carboxylate side chain of Glu 216 (Fig. 4a). The fluorine atoms in the aromatic CF_3 group are also potential H-bond acceptors for Ser 304 while the O atom of the picolinamide group is H-bonded with Thr 54. The CF_3-substituted phenyl ring formed hydrophobic/π-π interactions with Phe 120, whereas the central aromatic system of SOR also formed π-π interactions with Phe 483. The picolinamide system in SOR also forms π-π interactions with the aromatic residues Phe 51, Phe 58, and Phe 481, while additional hydrophobic interactions involve Val 49, Leu 71, Leu 73, Val 78, Leu 121, Leu 213, Val 308, Leu 372, Val 374, and Ile 396. The docking of SOR in the 4WNU and 4WNV structures was very similar to 3TDA, although the orientation of the picolinamide system differed somewhat and further H-bonds between the amido oxygen and the hydroxyl group of Thr 375 and the amido nitrogen and the carboxylate of Glu 222 were possible. However, there were no interactions between Glu 216 and either SOR or SNO in the 4WNU and 4WNV structures.

From kinetic studies the interaction of CYP2D6 with SNO was of higher affinity than that with SOR. In accord with these findings additional binding interactions emerged from the SNO-CYP2D6 docking analysis, although these varied somewhat between the different crystal structures. The O atom of the *N*-oxide group of SNO was involved in H-bonding with Thr 54 in the 3TDA structure and with Thr 394 in the 4WNU and 4WNV structures. In addition, docking studies in different X-ray structures revealed differences in the orientation of the pyridine and the amido side chain of the picolinamide moiety of SNO/SOR. This could be due to altered conformations of side chain (e.g., Phe 481, Phe 483) and backbone (e.g., Val 49, Phe 51) residues in the active site. The estimated K_d values from Surflex analysis of the docking of SNO with CYP2D6 were greater than those for SOR in each the three structures (Table II). Although these model-derived values should be interpreted with caution because they are protein structure-dependent (24,44), this suggests that SNO interacts more efficiently than SOR with CYP2D6. It is also noteworthy that the sites of metabolism in SOR were ~ 20 Å from the heme moiety; this is in agreement with the lack of SOR biotransformation by CYP2D6.

The coadministration of SOR and a large number of other drugs is contraindicated due to the possibility of DDIs (https://www.drugs.com/drug-interactions/sorafenib-index.html); several of these other drugs are CYP2D6 substrates. At present, there is little information regarding the potential impact of SOR on the pharmacokinetics of these contraindicated drugs, but there is evidence that the incidence of adverse effects is increased. Recent studies have suggested that there may be potential interactions between SOR and other drugs that are eliminated, at least in part, by CYP2D6. Thus, SOR has been combined with the histone deacetylase inhibitor and CYP2D6 substrate panobinostat (45) in several clinical studies. One patient with advanced hepatocellular carcinoma received the combination (46,47). There was some evidence of improved efficacy, but treatment was terminated due to toxicity. This study was part of a larger clinical trial but no results have yet been reported (NCT00823290). In patients with advanced HCC another trial with the combination was also terminated due to severe dose-limiting toxicity after the enrolment of the first three patients (48; NCT00873002).

The proteasomal inhibitor bortezomib is metabolized in part by CYP2D6 (49). Three trials assessed this combination in patients with several cancers. NCT01534260 was a Phase I dose escalating study and Phase II maximum tolerated dose

study that enrolled 37 patients with acute myelogenous leukemia. The SOR/bortezomib combination produced serious toxicity in 18 of the patients and all but one experienced adverse effects, especially gastrointestinal and dermal toxicities, with neuropenia and fever also produced in some individuals. In NCT00536575, SOR and bortezomib were administered to patients with multiple myeloma. Eleven of 13 patients completed that study, although significant adverse effects again included blood disorders, hypertension, gastrointestinal disturbances, fatigue, and severe rashes. A third study evaluated SOR and bortezomib in patients with metastatic renal cell carcinoma (NCT01100242). All 17 patients completed the study but experienced significant adverse effects, including blood disorders, hypertension, gastrointestinal disorders, dermal toxicities, and neurological disorders; serious adverse events occurred in six subjects.

SOR has also been combined with endocrine agents, including the CYP2D6 substrate, tamoxifen, for the treatment of patients with breast cancer (50). Although the combination with tamoxifen was generally well tolerated, one patient discontinued treatment and three others required dose reductions because of adverse dermatological effects. The observed time to progression was greater than 6 months and the clinical benefit rate was 50%, which appeared promising, because single-agent SOR has limited activity in patients with metastatic breast cancer. However, a trial of SOR, tamoxifen and cisplatin in melanoma patients commenced in April 2007 but has not reported results and may have been discontinued (NCT00492505).

The pharmacokinetics of SOR are complex and exhibit extensive interindividual variation (6,7). The systemic availabilities of SOR and SNO are increased in some patients who received prolonged therapy with the drug (4,6–9). Indeed, the maximal serum concentration (C_{max}) of SNO reportedly reached 8.5 μM in one patient, which is several-fold greater than the K_i for CYP2D6 inhibition that was estimated in the present study (8). Several other studies have also reported that SNO can reach serum concentrations of 1–5 μM in some patients (7,51,52). Accordingly, there is the potential that SOR may elicit pharmacokinetic DDIs in patients who produce high concentrations of SNO. CYP3A4 selectively oxidizes SOR to SNO in human liver (5). Potential sources of variation in the activity of the enzyme in vivo include genetic polymorphisms and exposure to coadministered drugs and other xenobiotics that are potent inhibitors and inducers (53). In addition, CYP3A4 function is greater in females and decreased in liver disease, which has been shown to impair the oxidation of SOR to SNO (53,54). These factors are likely to impact on the pharmacokinetics of SOR and the production of SNO. It would now be of interest to evaluate these possibilities directly in clinical studies.

CONCLUSIONS

The present study suggests that SNO is more potent than SOR as an inhibitor of CYP2D6. In docking studies, SOR interacted with multiple amino acid residues in CYP2D6, including putative SRS (37,55). The *N*-oxide moiety of SNO was involved in additional interactions, which is consistent with its greater inhibitory potency. SOR continues to be evaluated in combination with other anticancer and adjunct treatments in patients. However, the drug is contraindicated with a large number of agents and some clinical trials of such combinations have been terminated because of a high incidence of adverse effects. Whether this is due to pharmacokinetic DDIs has not been established. To complement the present study, it would now be of interest to assess SNO production directly in patients who are receiving drug combinations containing SOR. Moreover, serum SNO monitoring during therapy may enable individual patients to be identified who might benefit from drug regimen modifications in order to avoid SOR-mediated DDIs.

ACKNOWLEDGMENTS

Technical contributions in aspects of the study from Dr. S. Cui and Ms. K Bourget are also acknowledged. The supply of the human liver samples used in this study by Dr. J George is also gratefully acknowledged.

FUNDING INFORMATION

This study is financially supported by the Cancer Council NSW (grants RG09-14 and IG11-33). PCN is supported by the Flinders Centre for Innovation in Cancer (FCIC) and Flinders Medical Centre (FMC) Foundation through an Early Career Research Grant.

COMPLIANCE WITH ETHICAL STANDARDS

Conflict of Interest The authors declare that they have no conflict of interest.

REFERENCES

1. Escudier B, Eisen T, Stadler WM, Szczylik C, Oudard S, Siebels M, et al. Sorafenib in advanced clear-cell renal-cell carcinoma. New Engl J Med. 2007;356:125–34. https://doi.org/10.1056/NEJMoa060655.
2. Liu L, Cao Y, Chen C, Zhang X, McNabola A, Wilkie D, et al. Sorafenib blocks the RAF/MEK/ERK pathway, inhibits tumor angiogenesis, and induces tumor cell apoptosis in hepatocellular carcinoma model PLC/PRF/5. Cancer Res. 2006;66:11851–8. https://doi.org/10.1158/0008-5472.CAN-06-1377.
3. Awada A, Hendlisz A, Christensen O, Lathia CD, Bartholomeus S, Lebrun F, et al. Phase I trial to investigate the safety, pharmacokinetics and efficacy of sorafenib combined with docetaxel in patients with advanced refractory solid tumours. Eur J Cancer. 2012;48:465–74. https://doi.org/10.1016/j.ejca.2011.12.026.
4. Lathia C, Lettieri J, Cihon F, Gallentine M, Radtke M, Sundaresan P. Lack of effect of ketoconazole-mediated CYP3A inhibition on sorafenib clinical pharmacokinetics. Cancer Chemother Pharmacol. 2006;57:685–92. https://doi.org/10.1007/s00280-005-0068-6.
5. Ghassabian S, Rawling T, Zhou F, Doddareddy MR, Tattam BN, Hibbs DE, et al. Role of human CYP3A4 in the biotransformation of sorafenib to its major oxidized metabolites. Biochem Pharmacol. 2012;84:215–23. https://doi.org/10.1016/j.bcp.2012.04.001.
6. Strumberg D, Clark JW, Awada A, Moore MJ, Richly H, Hendlisz A, et al. Safety, pharmacokinetics, and preliminary antitumor activity of sorafenib: a review of four phase I trials in patients with advanced refractory solid tumors. Oncologist. 2007;12:426–37. https://doi.org/10.1634/theoncologist.12-4-426.
7. Minami H, Kawada K, Ebi H, Kitagawa K, Kim YI, Araki K, et al. Phase I and pharmacokinetic study of sorafenib, an oral multikinase inhibitor, in Japanese patients with advanced

refractory solid tumors. Cancer Sci. 2008;99:1492–8. https://doi.org/10.1111/j.1349-7006.2008.00837.x.
8. Inaba H, Rubnitz JE, Coustan-Smith E, Li L, Furmanski BD, Mascara GP, et al. Phase I pharmacokinetic and pharmacodynamic study of the multikinase inhibitor sorafenib in combination with clofarabine and cytarabine in pediatric relapsed/refractory leukemia. J Clin Oncol. 2011;29:3293–300. https://doi.org/10.1200/JCO.2011.34.7427.
9. Ferrario C, Strepponi I, Esfahani K, Charamis H, Langleben A, Scarpi E, et al. Phase I/II trial of sorafenib in combination with vinorelbine as first-line chemotherapy for metastatic breast cancer. PLoS One. 2016;11:e0167906. https://doi.org/10.1371/journal.pone.0167906.
10. Ghassabian S, Gillani TB, Rawling T, Crettol S, Nair PC, Murray M. Sorafenib N-oxide is an inhibitor of human hepatic CYP3A4. AAPS J. 2019;21:15. https://doi.org/10.1208/s12248-018-0262-1.
11. Gillani T, Rawling T, Murray M. Cytochrome P450-mediated biotransformation of sorafenib and its *N*-oxide metabolite: implications for cell viability and human toxicity. Chem Res Toxicol. 2015;28:92–102. https://doi.org/10.1021/tx500373g.
12. Murray M, Wilkinson CF, Marcus C, Dube CE. Structure-activity relationships in the interactions of alkoxymethylenedioxybenzene derivatives with rat hepatic microsomal mixed-function oxidases *in vivo*. Mol Pharmacol. 1983;24:129–36.
13. Cantrill E, Murray M, Mehta I, Farrell GC. Down-regulation of the male-specific steroid 16α-hydroxylase, cytochrome $P\text{-}450_{UT\text{-}A}$, in male rats with portal bypass: relevance to estradiol accumulation and impaired drug metabolism in hepatic cirrhosis. J Clin Invest. 1989;83:1211–6. https://doi.org/10.1172/JCI114003.
14. Ghassabian S, Chetty M, Tattam BN, Glen J, Rahme J, Stankovic Z, et al. A high-throughput assay using liquid chromatography/tandem mass spectrometry for simultaneous in vivo phenotyping of five major cytochrome P450 enzymes in patients. Ther Drug Monit. 2009;31:239–46. https://doi.org/10.1097/FTD.0b013e318197e1bf.
15. Murray M. Metabolite intermediate complexation of microsomal cytochrome P450 2C11 in male rat liver by nortriptyline. Mol Pharmacol. 1992;42:931–8.
16. Johnston RA, Rawling T, Chan T, Zhou F, Murray M. Selective inhibition of human solute carrier transporters by multikinase inhibitors. Drug Metab Dispos. 2014;42:1851–7. https://doi.org/10.1124/dmd.114.059097.
17. von Moltke LL, Greenblatt DJ, Cotreau-Bibbo MM, Duan SX, Harmatz JS, Shader RI. Inhibition of desipramine hydroxylation in vitro by serotonin-reuptake-inhibitor antidepressants, and by quinidine and ketoconazole: a model system to predict drug interactions in vivo. J Pharmacol Exp Ther. 1994;268:1278–83.
18. Fiser A, Sali A. ModLoop: automated modeling of loops in protein structures. Bioinformatics. 2003;19:2500–1. https://doi.org/10.1093/bioinformatics/btg362.
19. Gasteiger J, Marsili M. Iterative partial equalization of orbital electronegativity—a rapid access to atomic charges. Tetrahedron. 1980;36:3219–28. https://doi.org/10.1016/0040-4020(80)80168-2.
20. Powell MJD. Restart procedures for the conjugate gradient method. Math Program. 1977;12:241–54. https://doi.org/10.1007/BF01593790.
21. Clark M, Cramer RD III, Van Opdenbosch N. Validation of the general purpose tripos 5.2 force field. J Comput Chem. 1989;10:982–1012. https://doi.org/10.1002/jcc.540100804.
22. Jain AN. Surflex: fully automatic flexible molecular docking using a molecular similarity-based search engine. J Med Chem. 2003;46:499–511. https://doi.org/10.1021/jm020406h.
23. Nair PC, McKinnon RA, Miners JO. Computational prediction of the site(s) of metabolism and binding modes of protein kinase inhibitors metabolized by CYP3A4. Drug Metab Dispos. 2019;47:616–31. https://doi.org/10.1124/dmd.118.085167.
24. Pham TA, Jain AN. Parameter estimation for scoring protein-ligand interactions using negative training data. J Med Chem. 2006;49:5856–68. https://doi.org/10.1021/jm050040j.
25. Dayer P, Leemann T, Striberni R. Dextromethorphan O-demethylation in liver microsomes as a prototype reaction to monitor cytochrome P-450 db1 activity. Clin Pharmacol Ther. 1989;45:34–40. https://doi.org/10.1038/clpt.1989.6.
26. Marcus CB, Murray M, Wilkinson CF. Spectral and inhibitory interactions of methylenedioxyphenyl and related compounds with purified isozymes of cytochrome P-450. Xenobiotica. 1985;15:351–62. https://doi.org/10.3109/00498258509045370.
27. Butler AM, Murray M. Inhibition and inactivation of constitutive cytochromes P450 in rat liver by parathion. Mol Pharmacol. 1993;43:902–8.
28. Ortiz de Montellano PR, Correia MA. Suicidal destruction of cytochrome P-450 during oxidative drug metabolism. Annu Rev Pharmacol Toxicol. 1983;23:481–503. https://doi.org/10.1146/annurev.pa.23.040183.002405.
29. He K, Iyer KR, Hayes RN, Sinz MW, Woolf T, Hollenberg PF. Inactivation of cytochrome P450 3A4 by bergamottin, a component of grapefruit juice. Chem Res Toxicol. 1998;11:252–9. https://doi.org/10.1021/tx970192k.
30. Stupans I, Murray M, Kirlich A, Tuck K, Hayball P. Inactivation of cytochrome P450 by the food-derived complex phenol oleuropein. Food Chem Toxicol. 2001;39:1119–24. https://doi.org/10.1016/S0278-6915(01)00060-6.
31. Murray M. Complexation of cytochrome P-450 isoenzymes in hepatic microsomes from SKF 525-A-induced rats. Arch Biochem Biophys. 1988;262:381–8. https://doi.org/10.1016/0003-9861(88)90202-0.
32. Murray M, Field SL. Inhibition and metabolite complexation of rat hepatic microsomal cytochrome P450 by tricyclic antidepressants. Biochem Pharmacol. 1992;43:2065–71. https://doi.org/10.1016/0006-2952(92)90163-D.
33. Murray M. In vitro effects of quinoline derivatives on cytochrome P-450 and aminopyrine N-demethylase activity in rat hepatic microsomes. Biochem Pharmacol. 1984;33:3277–81. https://doi.org/10.1016/0006-2952(84)90090-X.
34. Nemeroff CB, DeVane CL, Pollock BG. Newer antidepressants and the cytochrome P450 system. Am J Psychiatr. 1996;153:311–20. https://doi.org/10.1176/ajp.153.3.311.
35. Ohyama K, Nakajima M, Suzuki M, Shimada N, Yamazaki H, Yokoi T. Inhibitory effects of amiodarone and its N-deethylated metabolite on human cytochrome P450 activities: prediction of in vivo drug interactions. Br J Clin Pharmacol. 2000;49:244–53. https://doi.org/10.1046/j.1365-2125.2000.00134.x.
36. Giri P, Naidu S, Patel N, Patel H, Srinivas NR. Evaluation of in vitro cytochrome P450 inhibition and in vitro fate of structurally diverse N-oxide metabolites: case studies with clozapine, levofloxacin, roflumilast, voriconazole and zopiclone. Eur J Drug Metab Pharmacokinet. 2017;42:677–88. https://doi.org/10.1007/s13318-016-0385-7.
37. Rodrigues AD. Measurement of human liver microsomal cytochrome P450 2D6 activity using [O-methyl-14C] dextromethorphan as substrate. Methods Enzymol. 1996;272:186–95. https://doi.org/10.1016/s0076-6879(96)72023-2.
38. Fowler S, Zhang H. In vitro evaluation of reversible and irreversible cytochrome P450 inhibition: current status on methodologies and their utility for predicting drug-drug interactions. AAPS J. 2008;10:410–23. https://doi.org/10.1208/s12248-008-9042-7.
39. Gotoh O. Substrate recognition sites in cytochrome P450 family 2 (CYP2) proteins inferred from comparative analyses of amino acid and coding nucleotide sequences. J Biol Chem. 1992;267:83–90.
40. Bapiro TE, Hasler JA, Ridderström M, Masimirembwa CM. The molecular and enzyme kinetic basis for the diminished activity of the cytochrome P450 2D6.17 (CYP2D6.17) variant. Potential implications for CYP2D6 phenotyping studies and the clinical use of CYP2D6 substrate drugs in some African populations. Biochem Pharmacol. 2002;64:1387–98. https://doi.org/10.1016/s0006-2952(02)01351-5.
41. Venhorst J, ter Laak AM, Commandeur JN, Funae Y, Hiroi T, Vermeulen NP. Homology modeling of rat and human cytochrome P450 2D (CYP2D) isoforms and computational rationalization of experimental ligand-binding specificities. J Med Chem. 2003;46:74–86. https://doi.org/10.1021/jm0209578.
42. Rowland P, Blaney FE, Smyth MG, Jones JJ, Leydon VR, Oxbrow AK, et al. Crystal structure of human cytochrome P450

2D6. J Biol Chem. 2006;281:7614–22. https://doi.org/10.1074/jbc.M511232200.
43. Maréchal JD, Kemp CA, Roberts GC, Paine MJ, Wolf CR, Sutcliffe MJ. Insights into drug metabolism by cytochromes P450 from modelling studies of CYP2D6-drug interactions. Br J Pharmacol. 2008;153(Suppl 1):S82–9. https://doi.org/10.1038/sj.bjp.0707570.
44. Ferrara P, Gohlke H, Price DJ, Klebe G, Brooks CL 3rd. Assessing scoring functions for protein-ligand interactions. J Med Chem. 2004;47:3032–47. https://doi.org/10.1021/jm030489h.
45. Clive S, Woo MM, Nydam T, Kelly L, Squier M, Kagan M. Characterizing the disposition, metabolism, and excretion of an orally active pan-deacetylase inhibitor, panobinostat, via trace radiolabeled ^{14}C material in advanced cancer patients. Cancer Chemother Pharmacol. 2012;70:513–22. https://doi.org/10.1007/s00280-012-1940-9.
46. Knieling F, Waldner MJ, Goertz RS, Strobel D. Quantification of dynamic contrast-enhanced ultrasound in HCC: prediction of response to a new combination therapy of sorafenib and panobinostat in advanced hepatocellular carcinoma. BMJ Case Rep. 2012;2012:bcr2012007576. https://doi.org/10.1136/bcr-2012-007576.
47. Gahr S, Wissniowski T, Zopf S, Strobel D, Pustowka A, Ocker M. Combination of the deacetylase inhibitor panobinostat and the multi-kinase inhibitor sorafenib for the treatment of metastatic hepatocellular carcinoma - review of the underlying molecular mechanisms and first case report. J Cancer. 2012;3:158–65. https://doi.org/10.7150/jca.4211.
48. Tsilimigras DI, Ntanasis-Stathopoulos I, Moris D, Spartalis E, Pawlik TM. Histone deacetylase inhibitors in hepatocellular carcinoma: a therapeutic perspective. Surg Oncol. 2018;27:611–8. https://doi.org/10.1016/j.suronc.2018.07.015.
49. Uttamsingh V, Lu C, Miwa G, Gan LS. Relative contributions of the five major human cytochromes P450, 1A2, 2C9, 2C19, 2D6, and 3A4, to the hepatic metabolism of the proteasome inhibitor bortezomib. Drug Metab Dispos. 2005;33:1723–8. https://doi.org/10.1124/dmd.105.005710.
50. Massarweh S, Moss J, Wang C, Romond E, Slone S, Weiss H, et al. Impact of adding the multikinase inhibitor sorafenib to endocrine therapy in metastatic estrogen receptor-positive breast cancer. Future Oncol. 2014;10:2435–48. https://doi.org/10.2217/fon.14.99.
51. Miller AA, Murry DJ, Owzar K, Hollis DR, Kennedy EB, Abou-Alfa G, et al. Phase I and pharmacokinetic study of sorafenib in patients with hepatic or renal dysfunction: CALGB 60301. J Clin Oncol. 2009;27:1800–5. https://doi.org/10.1200/JCO.2008.20.0931.
52. Flaherty KT, Lathia C, Frye RF, Schuchter L, Redlinger M, Rosen M, et al. Interaction of sorafenib and cytochrome P450 isoenzymes in patients with advanced melanoma: a phase I/II pharmacokinetic interaction study. Cancer Chemother Pharmacol. 2011;68:1111–8. https://doi.org/10.1007/s00280-011-1585-0.
53. Zanger UM, Schwab M. Cytochrome P450 enzymes in drug metabolism: regulation of gene expression, enzyme activities, and impact of genetic variation. Pharmacol Ther. 2013;138:103–41. https://doi.org/10.1016/j.pharmthera.2012.12.007.
54. Murray M, Gillani TB, Ghassabian S, Edwards RJ, Rawling T. Differential effects of hepatic cirrhosis on the intrinsic clearances of sorafenib and imatinib by CYPs in human liver. Eur J Pharm Sci. 2018;114:55–63. https://doi.org/10.1016/j.ejps.2017.12.003.
55. Nair PC, McKinnon RA, Miners JO. Cytochrome P450 structure-function: insights from molecular dynamics simulations. Drug Metab Rev. 2016;48:434–52. https://doi.org/10.1080/03602532.2016.1178771.